A Clinical Theory-Driven Deep Learning Model for Interpretable Autism Severity Prediction

Xiyang Hu
Arizona State University, xiyanghu@asu.edu

Abstract. Autism spectrum disorder (ASD) affects a substantial proportion of children worldwide, yet clinical assessment of symptom severity remains resource-intensive and unevenly accessible. Artificial intelligence (AI) has transformative potential to support scalable and timely severity assessment from behavioral data, but existing approaches largely treat autism as a monolithic prediction target and rely on opaque models that are difficult for clinicians to interpret or trust. Moreover, prior multimodal methods typically integrate heterogeneous behavioral signals using ad hoc fusion strategies that are weakly grounded in clinical theory. We propose a clinical theory-driven deep learning model for interpretable autism severity assessment that explicitly operationalizes established clinical constructs into model design. Drawing on autism research, we represent social communication deficits, motor control impairments, and gait abnormalities as distinct latent components. These components are integrated through a structured cross-modal attention mechanism guided by a learnable alignment mask that encodes soft spatial correspondence priors between visual and kinematic representations. The model further learns instance-specific theory weights that decompose each severity prediction into interpretable contributions from the three clinical domains, yielding transparent symptom profiles aligned with clinical reasoning. Comprehensive experiments demonstrate the state-of-the-art performance of our model over existing baselines. Ablation studies validate that performance gains arise from theory-driven design choices. Analysis of the learned theory weights reveals systematic relationships between symptom profiles and severity, providing empirical support for the multidimensional structure of autism. This work demonstrates how clinical theory can be instantiated as empirically testable architectural designs in deep learning models, advancing both predictive utility and interpretability in healthcare AI systems.

Key words: Autism spectrum disorder, Deep learning, Theory-driven design, Interpretable machine learning, AI for health

1. Introduction

Autism spectrum disorder (ASD) represents one of the most significant neurodevelopmental conditions affecting children worldwide, with profound implications for individuals, healthcare systems, and society at large. The condition is characterized by persistent challenges in social communication and interaction, alongside restricted and repetitive patterns of behavior, interests, or activities (Guha 2014). Early and accurate

identification of autism severity is critical because it directly informs the intensity and type of interventions a child receives, and research consistently demonstrates that early intervention leads to significantly improved developmental trajectories (Dawson et al. 2010). Yet the diagnostic process remains resource-intensive and inequitable: the gold-standard assessment instrument, the Autism Diagnostic Observation Schedule (ADOS, Lord et al. 2000), requires administration by extensively trained clinicians over 40 to 60 minutes of structured interaction, followed by detailed coding and interpretation. This bottleneck, with diagnostic evaluation wait times extending to 12 to 18 months in many regions, causes many children to miss critical early intervention windows, leading to long-term consequences for development and quality of life.

Recent advances in artificial intelligence (AI) offer a promising pathway to mitigate these diagnostic bottlenecks by augmenting or partially automating aspects of autism assessment. By systematically analyzing observed behavior, AI-based systems have the potential to support scalable screening, triage, and clinical decision support, particularly in resource-constrained clinical settings (Morrow et al. 2023). A growing body of work has applied machine learning and deep learning methods to autism-related tasks using video, audio, or motion data, reporting encouraging results in severity estimation and diagnostic classification (Zahan et al. 2023, Bae et al. 2025). Despite this progress, existing approaches exhibit fundamental limitations that restrict both their practical effectiveness and their readiness for integration into clinical workflows.

First, most AI-based autism assessment models treat severity as a single, undifferentiated prediction target. Behavioral signals are processed through generic architectures optimized primarily for prediction accuracy, without explicit consideration of how different symptom domains contribute to severity (Cavus et al. 2021). This stands in contrast to clinical assessment, where clinicians interpret observed behaviors through established theoretical constructs, including social communication deficits (Chevallier et al. 2012), motor coordination difficulties (Fournier et al. 2010, Gowen and Hamilton 2013), and gait abnormalities (Esposito et al. 2011, Lum et al. 2021). Clinicians then integrate evidence across these domains to form severity judgments. When computational models ignore this structure, they risk capturing spurious correlations, lack the flexibility to adapt to heterogeneous symptom profiles, and provide limited insights into understanding of autism heterogeneity. Second, many existing models operate as black boxes. Although post hoc explanation

techniques are sometimes applied, these explanations are often weakly connected to clinical concepts and difficult for clinicians to verify. In high-stakes healthcare contexts, lack of transparency poses a significant barrier to adoption (Rudin 2019, Durán and Jongsma 2021), as clinicians must be able to understand, evaluate, and contextualize algorithmic recommendations within their own reasoning processes. Models that produce accurate but opaque predictions provide limited value as clinical decision support tools. Third, prior multimodal approaches frequently rely on naive fusion strategies, such as feature concatenation, that do not reflect the semantic relationships between heterogeneous behavioral modalities (Zahan et al. 2023). Visual appearance and body movement, for example, capture complementary but structurally related information. Treating these modalities as interchangeable feature representations ignores their inherent asymmetries and limits a model's capacity to integrate evidence in a manner consistent with clinical reasoning.

In this study, we propose a novel clinical theory-driven deep learning model for interpretable autism severity prediction. Rather than treating autism severity as a monolithic outcome, our model explicitly encodes three established clinical constructs, namely social communication deficits, motor control impairments, and gait abnormalities, as distinct latent components. Each construct is derived from the behavioral modality that most naturally affords its measurement, reflecting clinical assessment practice. Visual representations capture appearance-based cues relevant to social communication, while kinematic representations capture movement dynamics associated with motor control and gait. To integrate these components, we introduce a structured cross-modal attention mechanism in which visual features provide contextual queries over kinematic representations. This integration is guided by a learnable alignment mask that encodes soft spatial correspondence priors between image regions and skeletal joints, balancing domain knowledge with data-driven adaptation. Importantly, the model learns instance-specific theory weights that quantify the contribution of each clinical construct to predicted severity. These weights produce interpretable symptom profiles that decompose predictions into clinically meaningful components, enabling transparency by design rather than post hoc explanation.

We evaluate the proposed model using a publicly available autism assessment dataset derived from standardized clinical interactions. Empirical results show that our model achieves state-of-the-art predictive

performance while providing clinically transparent outputs. Through controlled ablation studies, we demonstrate that performance gains stem from theory-driven design choices rather than increased model complexity. Analysis of the learned theory weights further reveals systematic relationships between symptom profiles and severity, consistent with clinically observed heterogeneity across behavioral domains. These results provide empirical support for the multidimensional and heterogeneous structure of autism symptomatology in clinical theory, and demonstrate that our model not only predicts severity accurately but also recovers clinically meaningful structure that aligns with established clinical practices and theoretical expectations.

This work makes multiple contributions. First, we present the first model architecture that explicitly operationalizes established clinical theories of autism as structural components of a multimodal deep learning system, demonstrating that theory-driven design can simultaneously improve predictive performance and interpretability. Rather than relying on post-hoc explanation, our approach encodes clinical constructs directly into the model, yielding transparent, construct-level symptom representations. Second, we make a theoretical contribution by showing that clinical theories can be instantiated as empirically testable architectural designs. Through systematic ablation, we evaluate core theoretical assumptions about the relative roles of social communication, motor control, and gait in autism severity, moving beyond descriptive theory toward falsifiable computational instantiations. Third, we deliver a practical clinical decision support framework that achieves state-of-the-art predictive accuracy while producing interpretable, instance-specific symptom profiles that clinicians can directly relate to observed behavior. By enabling clinicians to inspect how different symptom domains contribute to severity estimates for each individual, the system supports trust calibration, individualized intervention planning, and integration with existing clinical workflows. Together, these contributions establish a new paradigm for autism assessment systems, in which computational models do not merely predict outcomes, but instantiate clinical theory, support clinical reasoning, and generate testable insights into symptom heterogeneity.

2. Related Work

2.1. Clinical Theories of Autism

Autism spectrum disorder is clinically defined by deficits in social communication and the presence of restricted, repetitive behaviors (Guha 2014). Recent research increasingly emphasizes autism as a multidimensional condition with motor and gait-related differences that extend beyond the diagnostic core (Fournier

et al. 2010, Lum et al. 2021). We focus on three theoretically grounded behavioral constructs that serve as conceptual building blocks for our architecture: social communication, motor control, and gait.

Social Communication Deficits. Impairments in social interaction constitute a hallmark of autism, encompassing reduced eye contact, atypical facial expressions, diminished reciprocal gestures, and unusual body posture during social exchanges (Rutter et al. 2012, Lord et al. 2000). The social motivation theory (Chevallier et al. 2012) proposes that these deficits reflect reduced intrinsic interest in social stimuli, linked to abnormalities in brain reward systems. Clinically, assessment protocols like ADOS (Lord et al. 2000, Rutter et al. 2012) heavily emphasize observation of these social-communicative behaviors, making them central targets for computational modeling. Our architecture operationalizes this construct through visual features extracted from visual representations, which preserve appearance-based cues related to body posture, spatial orientation, and movement context relevant to social communication.

Motor Control Impairments. Motor coordination difficulties affect 50–80% of individuals with autism (Fournier et al. 2010, Kangarani-Farahani et al. 2024), including deficits in fine motor skills, manual dexterity, balance, and bilateral coordination. Importantly, motor impairments correlate with core autism symptom severity (Gowen and Hamilton 2013, MacDonald et al. 2013), suggesting they are not merely comorbid but may reflect shared underlying neurological factors. From a computational perspective, kinematic features capturing joint coordination patterns and movement smoothness provide direct measurements of motor control. Our model explicitly represents motor control as a distinct latent channel derived from skeletal joint trajectories, enabling empirical assessment of its incremental contribution to severity prediction.

Gait Abnormalities. Recent research identifies gait patterns as promising behavioral biomarkers for autism (Esposito et al. 2011, Kindregan et al. 2015). Documented abnormalities include increased step width, reduced step length, greater stride variability, and asymmetric bilateral coordination (Lum et al. 2021). Unlike motor control (which encompasses diverse movement types), gait focuses specifically on locomotion patterns that may reveal distinct neuromotor signatures. By isolating gait as a separate theoretical construct within our architecture, we enable empirical testing of whether locomotion-specific features provide incremental predictive value beyond general motor coordination.

These three theoretical constructs form the conceptual foundation of our architecture, distinguishing it from atheoretical approaches that treat autism as a monolithic classification target without internal structure.

2.2. Computational Methods for Autism Assessment

The application of machine learning to autism assessment has evolved from traditional feature engineering approaches to modern deep learning methods, with recent work exploring multimodal integration.

Traditional Machine Learning with Handcrafted Features. Early computational approaches relied on expert-designed features extracted from behavioral observations, physiological sensors, or demographic data, combined with classical supervised learning algorithms (e.g., logistic regression, rule induction, decision trees, support vector machines, random forests) (Wall et al. 2012, Duda et al. 2016). While these methods may benefit from interpretability and data efficiency, their performance is bounded by the quality and completeness of manually engineered features. They also struggle to capture complex, hierarchical patterns in high-dimensional behavioral data such as video sequences. Our experiments include traditional ML baselines to establish whether deep learning provides tangible improvements over expert feature engineering.

Single-Modality Deep Learning. Recent work applies deep neural networks to autism-related prediction tasks using individual data modalities. Convolutional neural networks (CNNs) have been used for facial expression analysis, while recurrent neural networks (RNNs) and graph convolutional networks (GCNs) have been applied to time-series physiological data and skeletal motion sequences. Pose-based models capture motor patterns (Zhang et al. 2021), video-based methods detect affective and social cues (Hashemi et al. 2018), and acoustic models extract speech prosody (Bone et al. 2016). These approaches achieve impressive performance on specific modalities but ignore the complementary information available from multimodal observations. Our single-modality baselines test whether multimodal integration is helpful for this task.

Multimodal Learning for Autism. A growing body of work recognizes that autism manifests through multiple observable channels, motivating multimodal approaches. Tariq et al. (2018) used smartphone videos and behavioral ratings for autism classification. More recent methods align text, audio, and video cues for early screening (Zhu et al. 2023, Bae et al. 2025). Zahan et al. (2023) proposed a state-of-the-art multimodal method combining visual and kinematic data for autism detection, demonstrating performance improvements over single-modality approaches. However, for all these methods, behavioral signals from different modalities are typically fused through feature concatenation or late-stage aggregation, without

explicit modeling of the semantic relationships between modalities or aligning model structure with clinical constructs. As a result, these models provide limited insight into how different symptom domains contribute to severity estimates and offer little support for understanding symptom heterogeneity. Our work advances these by introducing cross-attention for semantic correspondence learning and theory-guided architecture design for interpretable, clinically grounded integration.

2.3. Theory-Driven and Interpretable AI in Healthcare

Our work also contributes to the call for theory-driven design of AI algorithms, particularly in high-stakes domains like healthcare where interpretability and trust are paramount.

Interpretable Machine Learning for Clinical Decision Support. The black box nature of deep learning poses challenges for clinical adoption, where predictions must be explainable to support decision-making and ensure accountability (Durán and Jongsma 2021, Ahmed et al. 2023). Interpretable ML methods, including attention visualization, saliency maps, concept-based explanations, and inherently interpretable architectures, aim to open these black boxes (Rudin et al. 2022). However, many interpretability techniques are completely *post-hoc* (explaining existing models after training) rather than *by-design* (building interpretability into architecture), which have concerning reliability limitations (Rudin 2019). Our approach embodies interpretability-by-design: theoretical constructs are explicit latent channels, and learnable theory weights provide instance-specific explanations in terms of clinically meaningful symptom dimensions. These ensures predictions are not only accurate but also *intelligible* to clinicians and *grounded* in established theories.

Theory-Driven Model Design for Healthcare AI. Recent research has increasingly incorporated medical and behavioral theory into the design of healthcare algorithms. By organizing model architectures around medical meaningful constructs, these approaches seek to improve both predictive performance and interpretability. For instance, Xie et al. (2025) propose a knowledge-guided neural topic model that incorporates medically grounded seed terms to predict the mental health effects of online video content. Li et al. (2025) introduce a large language model multi-agent framework for drug discovery that is guided by organizational theories of cognitive labor and iterative learning, supporting coordinated agent collaboration with biomedical knowledge grounding. Zhou et al. (2023) develop a multi-armed bandit algorithm for personalized health

intervention recommendation, where diversity promotion is informed by behavioral theory. Morid and Sheng (2025) present a channel-wise deep learning model for patient cost prediction that structures inputs by distinct categories of medical codes, addressing both data heterogeneity and sociotechnical fairness. Lin et al. (2017) propose a multitask learning framework for chronic care risk profiling, where each task corresponds to a specific adverse outcome and shared structure supports joint clinical inference. Our model follows this line of work by aligning modality-specific channels with behavioral constructs derived from autism theory.

3. Methodology

3.1. Task Definition

We study the problem of predicting autism severity from *temporal skeleton sequences*, which represent body joint positions over time. In many clinical and research settings, raw video recordings of behavioral assessments are not available for downstream modeling. Due to privacy regulations governing sensitive recordings of children, including HIPAA and GDPR, video data are often not released in their original form and are instead transformed into privacy-reduced representations suitable for analysis (Ahmed et al. 2023). Among these, skeleton sequences are widely used and commonly distributed in autism datasets, making skeleton-based modeling a prevalent practical setting (Billing et al. 2020). In addition to their availability, skeleton representations remove identifiable visual information such as facial appearance, clothing, and scene context while preserving kinematic structure relevant to behavior (Cao et al. 2019). This combination of practical accessibility and reduced privacy risk makes temporal skeleton sequences a common representation for autism assessment.

Formally, let y denote the ground-truth ADOS total score for an individual, where higher scores indicate greater symptom severity (Lord et al. 2000, Gotham et al. 2009). The ADOS total score aggregates assessments across multiple behavioral domains, including social affect, restricted and repetitive behaviors, and overall impression, making it a clinically validated summary measure of autism severity (Rutter et al. 2012). Our prediction task is formulated as a regression problem: given a skeleton temporal sequence $\mathcal{X} \in \mathbb{R}^{C \times T \times J}$ capturing an individual's movements during a standardized assessment session (where C denotes spatial coordinates, T denotes temporal frames, and J denotes body joints), predict the ADOS total score $\hat{y} \approx y$.

Following prior work (Zahan et al. 2023), we derive two complementary representations from the same underlying skeletal sequence. First, we retain $\mathcal{X}$ in its native form as *kinematic data*, which captures joint-level movement dynamics suitable for modeling motor control and gait. Second, we transform $\mathcal{X}$ into a *SKEPXEL pseudo-image* $\mathcal{I}$ via a skeleton-to-pixel projection (Liu et al. 2019), which encodes spatiotemporal joint trajectories into a two-dimensional visual format. This dual representation enables multimodal learning from a single privacy-preserving data source, while supporting different types of behavioral information.

3.2. Clinical Theory-Driven Design Rationale

Our model design is informed by clinical theory and practice. We summarize our high-level design rationale:

First, construct-level representation. Clinical assessment of autism severity distinguishes among multiple symptom domains, including social communication, motor coordination, and gait-related behaviors. Rather than treating behavioral data as undifferentiated input, we adopt a theory-driven approach that explicitly operationalizes three clinical constructs (*social*, *motor*, and *gait*) as distinct latent channels within the model architecture. This decomposition mirrors clinical reasoning, enables interpretable predictions by exposing each symptom dimension's contribution, and supports empirical analysis of which domains are most predictive.

Second, modality–construct alignment. Different behavioral domains are most naturally observed through different modalities. Appearance-based cues are central to assessing social communication behaviors, while joint kinematics provide direct evidence of motor control and gait. Accordingly, social communication is modeled from visual features derived from SKEPXEL pseudo-images that capture holistic body configurations, whereas motor control and gait are modeled from skeleton joint trajectories. This alignment grounds each construct in the observational channel that best supports its measurement in clinically meaningful ways.

Third, instance-specific interpretability under heterogeneity. Autism is characterized by substantial inter-individual variability, with different individuals exhibiting different patterns of strengths and impairments across symptom domains. To reflect this heterogeneity, the model learns instance-specific weights over the construct-level components rather than relying on fixed fusion rules. These learned weights indicate the relative contribution of social, motor, and gait dimensions to each individual's predicted severity and can be interpreted as personalized symptom profiles, mirroring how clinicians conceptualize autism heterogeneity.

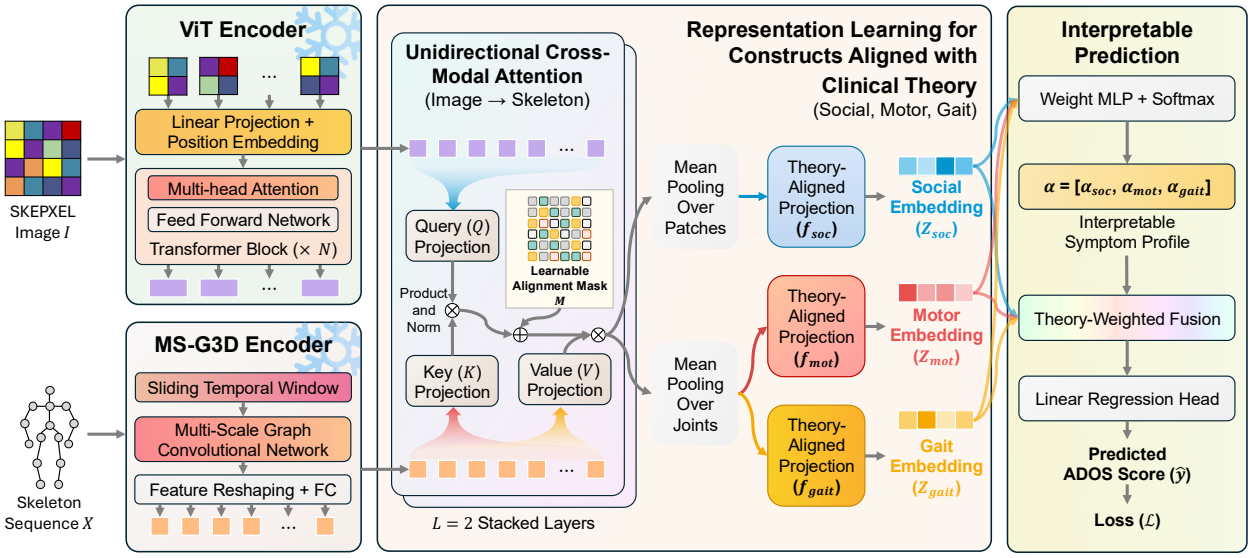

Figure 1 **Overview of the proposed theory-guided model architecture for autism severity prediction. A SKEPXEL pseudo-image and a skeleton sequence are encoded by frozen pretrained backbones (ViT and MS-G3D) into patch and joint tokens, which are aligned via unidirectional cross-attention from image patches to skeleton joints. A learnable alignment mask biases attention toward plausible joint to patch correspondences. The resulting representations are projected into three theory-aligned latent channels (social communication, motor control, gait), combined using instance-specific theory weights, and fused with an interaction term to produce the final severity estimate.**

Figure 1 illustrates our model architecture, which operationalizes the above principles through a modular separation of feature extraction and theory-guided integration. Visual and kinematic inputs are processed by frozen pretrained encoders, after which we learn three construct-specific latent channels corresponding to social communication, motor control, and gait. These channels are integrated through learnable, instance-specific weighting for severity prediction. We employ cross-modal attention mechanisms to allow effective information exchange between modalities, with a learnable alignment mask that encodes soft priors over spatial correspondence between image patches and skeleton joints, such as stronger coupling between head-region patches and head or neck joints. We present each component of the architecture in detail below.

3.3. Multimodal Feature Extraction: Frozen Domain-General Encoders

Given a multimodal input consisting of a skeleton sequence $\mathcal{X}$ and its corresponding visual representation $\mathcal{I}$, our model first performs feature extraction using frozen pretrained encoders. Each modality is transformed

into high-dimensional embeddings that capture kinematic and visual information at appropriate temporal and spatial resolutions. These embeddings are treated as fixed, semantically informative representations and are subsequently aligned and integrated by task-specific, theory-driven modules described in later subsections.

This design leverages large-scale pretrained models to provide robust and transferable feature extractors for graph-structured motion data and images, while concentrating learning capacity on the autism assessment–specific problem of interpreting and integrating these features in accordance with established clinical theories. At the same time, freezing the pretrained encoders sharply limits the number of trainable parameters, reducing the risk of overfitting on small clinical datasets. Such datasets are typically orders of magnitude smaller than those used for pretraining vision and action recognition models, making end-to-end fine-tuning prone to memorization rather than generalization.

3.3.1. Kinematic Encoder: MS-G3D Graph Convolutional Network for Skeleton Sequences

To extract kinematic features from the skeleton sequence $\mathcal{X}$, we employ a Multi-Scale Graph Convolutional Network with 3D convolutions (MS-G3D) (Liu et al. 2020), a state-of-the-art architecture specifically designed for skeleton-based action recognition. The MS-G3D model represents skeleton sequences as spatiotemporal graphs, where nodes correspond to body joints and edges encode physical connectivity (bone structure) and temporal links across frames.

Graph Representation. The skeleton graph is defined by a binary adjacency matrix that encodes the skeletal topology (e.g., the wrist is connected to the elbow, the elbow to the shoulder, etc.). This structural prior is essential for learning physically meaningful movement patterns, as it constrains the model to respect anatomical constraints when aggregating information across joints.

Multi-Scale Spatiotemporal Convolutions. The MS-G3D architecture applies graph convolutions at multiple spatial scales (capturing both local joint relationships and longer-range kinematic chains) and temporal scales (capturing both short-term motion dynamics and longer-term movement trends). The multi-scale design is motivated by the observation that different autism-related motor behaviors manifest at different spatiotemporal scales: for example, fine motor coordination may be reflected in localized, rapid joint movements, while gait asymmetry may be evident in longer-range, slower bilateral patterns.

After processing the input skeleton sequence $\mathcal{X}$ through multiple MS-G3D layers, the model produces a feature tensor with dimensions (N, d, T', J), where N is the batch size, d is the learned feature channel dimension, T' is the temporally downsampled time dimension, and J is the number of joints. To obtain joint-level embeddings suitable for cross-modal alignment, we perform temporal average pooling: $\boldsymbol{E}^{(0)}_{\text{skel,raw}} = \frac{1}{T'}\sum_{t=1}^{T'} \text{MSG3D}(\mathcal{X})[:,:,t,:] \in \mathbb{R}^{J\times d}$. This yields a set of J joint embeddings, each of dimensionality d, that encode the kinematic patterns associated with each body joint over the entire observed sequence.

Projection. We apply a trainable linear projection independently to each joint token: $\boldsymbol{E}^{(0)}_{\text{skel}} = \boldsymbol{E}^{(0)}_{\text{skel,raw}}\boldsymbol{W}_{\text{skel-proj}} \in \mathbb{R}^{J\times d}$. This projection functions as an alignment and adaptation layer, mapping pretrained kinematic representations into the shared latent space used by subsequent multimodal fusion modules.

From a theoretical perspective, the frozen MS-G3D encoder captures *kinematic behavioral features* that are directly relevant to motor control and gait assessment. The joint-level representations encode movement dynamics, coordination patterns, joint angle trajectories, and temporal rhythms that reflect underlying motor capabilities and locomotion characteristics.

3.3.2. Visual Encoder: Vision Transformer for SKEPXEL Images

To extract visual features from the SKEPXEL pseudo-images $\mathcal{I}$, we employ a Vision Transformer (ViT) architecture (Dosovitskiy et al. 2021). The ViT model processes images by partitioning them into a regular grid of non-overlapping patches, embedding each patch via a learned linear projection, and then applying a stack of Transformer encoder layers to capture global relationships among patches through self-attention.

Patch Tokenization. Given an input SKEPXEL image $\mathcal{I} \in \mathbb{R}^{H\times W\times 3}$, the ViT divides the image into a 14×14 grid, yielding $P = 196$ patches of size 16×16 pixels each. Each patch is flattened and linearly projected to produce a $D_{\text{ViT}} = 768$-dimensional embedding. After adding learned positional encodings (to preserve spatial structure) and passing through the ViT's Transformer encoder stack, the model outputs a set of patch-level embeddings: $\boldsymbol{E}^{(0)}_{\text{img,raw}} = \text{ViT}(\mathcal{I}) \in \mathbb{R}^{P\times D_{\text{ViT}}}$.

Projection. To support direct cross-modal interaction with joint-level kinematic tokens, we apply a learned linear projection to each visual patch embedding, mapping the ViT output from D_{ViT} into the shared latent space of dimension d: $\boldsymbol{E}^{(0)}_{\text{img}} = \boldsymbol{E}^{(0)}_{\text{img,raw}}\boldsymbol{W}_{\text{img-proj}} \in \mathbb{R}^{P\times d}$. This projection aligns appearance-based visual

features with the kinematic embedding space, enabling meaningful comparison, correspondence modeling, and fusion between visual patches and body joints in downstream multimodal attention mechanisms. The projection layer is trainable, allowing adaptation of pretrained ViT features to the SKEPXEL representation and the target behavioral assessment task.

From a theoretical perspective, the frozen ViT encoder captures *appearance-based behavioral cues* that are relevant to social communication assessment. The patch-level representations encode visual patterns such as body posture configurations, spatial orientations, head positions, and overall movement contexts. These visual features complement the more explicitly kinematic information provided by the skeleton encoder, enabling the model to integrate complementary perspectives on the same behavioral episode.

3.4. Cross-Modal Alignment via Unidirectional Attention: Image-to-Skeleton Information Flow

A critical challenge in multimodal fusion for autism assessment is aligning and integrating information from heterogeneous modalities, visual (patch-based image features) and kinematic (joint-based skeleton features), that represent complementary perspectives on the same behavioral episode. Our architecture addresses this through a unidirectional cross-attention mechanism in which *image patches query skeleton joints*, enabling visual contextual features to augment kinematic representations in a structured and interpretable manner.

3.4.1. Theoretical Motivation for Unidirectional Image-to-Skeleton Attention We design the attention flow from image to skeleton (rather than bidirectional or skeleton-to-image) based on the following clinical considerations:

First, visual appearance cues, such as overall body posture, spatial orientation relative to interaction partners, head position, and configurational patterns, provide rich contextual information that is highly relevant for assessing social communication deficits, a core dimension of autism symptomatology. By allowing image patches to query skeleton joints, the model can effectively ask: “Given the visual context, how should we interpret the kinematic patterns of specific joints?” This query direction aligns with clinical reasoning process (Guha 2014), where contextual visual cues inform the interpretation of specific movements.

Second, the SKEPXEL representation inherently encodes spatiotemporal patterns at a more global level compared to individual joint trajectories. Image patches capture not only individual joint configurations but

also their spatial relationships, movement trajectories over time, and overall movement "gestalt." Directing attention from this richer, more contextual modality (image) to the more local, anatomically structured modality (skeleton) allows the model to use global patterns to guide integration of local kinematic features.

Third, from a regularization perspective, unidirectional attention imposes a simpler, more constrained integration structure compared to bidirectional cross-attention, which may help prevent overfitting on small clinical datasets. By restricting information flow to a single direction, we reduce the number of trainable parameters and the complexity of cross-modal interactions, potentially improving generalization. Our experimental results (reported in §5.5) empirically validate this design choice, demonstrating that unidirectional image-to-skeleton attention outperforms both bidirectional and reverse-direction alternatives.

3.4.2. Learnable Alignment Mask: Encoding Spatial Correspondence Priors A key innovation in our cross-attention design is the introduction of a learnable alignment mask $\boldsymbol{M} \in \mathbb{R}^{J \times P}$ that acts as an additive bias on attention logits. This mask encodes soft priors over the correspondence between skeleton joints and image patches, reflecting certain joints naturally attend more strongly to specific image regions. Consider, for example, the correspondence between the head joint and the upper-center region of the image, or between hand joints and patches near the extremities. While these correspondences are not perfectly deterministic (they depend on body pose, camera viewpoint, and movement dynamics), they provide useful structural priors that guide the attention mechanism toward anatomically and spatially coherent alignments.

Learning vs. Imposing Correspondence. Rather than manually specifying these correspondences (which would require labor-intensive annotation and may not generalize across different pose configurations), we make the alignment mask $\boldsymbol{M}$ a *learnable parameter* of the model. The mask is initialized with small random values and updated via gradient descent during training, allowing the model to discover the most predictive correspondence patterns directly from the data. This design balances domain knowledge (spatial structure matters) with flexibility (let data determine the specific correspondences).

3.4.3. Multi-Layer Cross-Attention Architecture Our cross-modal integration module consists of $L = 2$ stacked cross-attention layers, enabling hierarchical refinement of multimodal representations. Let $\boldsymbol{E}_{\text{img}}^{(\ell)} \in \mathbb{R}^{P \times d}$ and $\boldsymbol{E}_{\text{skel}}^{(\ell)} \in \mathbb{R}^{J \times d}$ denote the patch and joint embeddings at layer $\ell \in \{0, 1, \ldots, L-1\}$, where $\boldsymbol{E}_{\text{img}}^{(0)}$ and $\boldsymbol{E}_{\text{skel}}^{(0)}$ are the outputs from the frozen ViT and MS-G3D encoders as defined above.

Cross-Attention from Image to Skeleton. At each layer ℓ, we compute cross-attention in which image patches query skeleton joints. First, we form query, key, and value projections: $\boldsymbol{Q} = \boldsymbol{E}_{\text{img}}^{(\ell)}\boldsymbol{W}_Q$, $\boldsymbol{K} = \boldsymbol{E}_{\text{skel}}^{(\ell)}\boldsymbol{W}_K$, $\boldsymbol{V} = \boldsymbol{E}_{\text{skel}}^{(\ell)}\boldsymbol{W}_V$, where $\boldsymbol{W}_Q, \boldsymbol{W}_K, \boldsymbol{W}_V \in \mathbb{R}^{d\times d_h}$ are learned projection matrices, and d_h is the dimensionality per attention head. We use multi-head attention with multiple parallel heads to capture diverse alignment patterns.

Next, we compute the attention weights with the learnable alignment mask:

$$\boldsymbol{A} = \text{softmax}\left(\frac{\boldsymbol{Q}\boldsymbol{K}^\top}{\sqrt{d_h}} + \boldsymbol{M}^\top\right) \in \mathbb{R}^{P\times J}. \tag{1}$$

The attention matrix $\boldsymbol{A}$ encodes, for each image patch, a distribution over skeleton joints indicating which joints are most relevant for interpreting that patch. The alignment mask $\boldsymbol{M}^\top$ biases these weights toward spatially and anatomically coherent correspondences.

Finally, we aggregate joint features to update patch embeddings: $\tilde{\boldsymbol{E}}_{\text{img}}^{(\ell)} = \boldsymbol{A}\boldsymbol{V} \in \mathbb{R}^{P\times d_h}$. After multi-head concatenation and output projection, the updated patch embeddings $\tilde{\boldsymbol{E}}_{\text{img}}^{(\ell)}$ are combined with residual connections and layer normalization (following standard Transformer design) to produce $\boldsymbol{E}_{\text{img}}^{(\ell+1)}$.

Self-Attention and Feed-Forward Layers. In addition to cross-attention, each layer also includes: (1) *Modality-specific self-attention* over image patches (allowing patches to contextualize each other within the visual modality) and over skeleton joints (allowing joints to contextualize each other within the kinematic modality). These self-attention operations preserve and refine within-modality coherence. (2) *Position-wise feed-forward networks* applied independently to each token (patch or joint), providing non-linear transformation capacity. (3) *Residual connections and layer normalization* around each sub-layer, ensuring stable gradient flow and facilitating deep architecture training.

Importantly, there is *no reverse cross-attention* from skeleton joints to image patches in this architecture. This unidirectional design constrains the information flow to align with our theoretical hypothesis about the role of visual context in augmenting kinematic interpretation. The empirical validation of this design choice, compared to bidirectional and reverse-direction alternatives, is presented in §5.5.

After $L = 2$ layers of cross-attention processing, we obtain final patch embeddings $\boldsymbol{E}_{\text{img}}^{(L)}$ and joint embeddings $\boldsymbol{E}_{\text{skel}}^{(L)}$ that are enriched with cross-modal information, ready for theory-guided fusion.

3.5. Theory-Guided Latent Decomposition and Interpretable Fusion

After the cross-attention layers align and integrate visual and kinematic modalities, the next stage of our architecture operationalizes the three theoretical constructs, namely social communication, motor control, and gait, as explicit latent channels. This theory-driven decomposition serves both predictive and interpretive functions: it structures the feature space according to clinically grounded dimensions, and enables instance-specific assessment of which symptom domains are most relevant for each individual's predicted severity.

3.5.1. Pooling and Modality-Level Representations First, we aggregate the token-level embeddings from the final cross-attention layer into modality-level vectors through pooling:

$$\bar{\boldsymbol{e}}_{\text{img}} = \text{MeanPool}(\boldsymbol{E}_{\text{img}}^{(L)}) = \frac{1}{P}\sum_{p=1}^{P} \boldsymbol{E}_{\text{img}}^{(L)}[p,:] \in \mathbb{R}^d, \ \bar{\boldsymbol{e}}_{\text{skel}} = \text{MeanPool}(\boldsymbol{E}_{\text{skel}}^{(L)}) = \frac{1}{J}\sum_{j=1}^{J} \boldsymbol{E}_{\text{skel}}^{(L)}[j,:] \in \mathbb{R}^d, \quad (2)$$

Mean pooling aggregates information across all patches (for the image modality) and all joints (for the skeleton modality), producing compact, fixed-size representations that summarize the multimodal behavioral patterns observed during the assessment session.

3.5.2. Theory-Aligned Projection Functions Next, we project these pooled representations into three theory-aligned latent channels, each corresponding to one of our theoretical constructs:

$$z_{\text{soc}} = f_{\text{soc}}(\bar{\boldsymbol{e}}_{\text{img}}) \in \mathbb{R}^{d_z}, \qquad \text{(Social)} \quad (3)$$

$$z_{\text{mot}} = f_{\text{mot}}(\bar{\boldsymbol{e}}_{\text{skel}}) \in \mathbb{R}^{d_z}, \qquad \text{(Motor)} \quad (4)$$

$$z_{\text{gait}} = f_{\text{gait}}(\bar{\boldsymbol{e}}_{\text{skel}}) \in \mathbb{R}^{d_z}, \qquad \text{(Gait)} \quad (5)$$

where d_z is the latent dimension (chosen to balance expressiveness and overfitting risk), and each $f_{\cdot}(\cdot)$ is a small multi-layer perceptron (MLP) with layer normalization and dropout for regularization.

Modality-Construct Alignment. The mapping of constructs to modalities reflects our theoretical understanding of which observational channels most naturally afford the measurement of each symptom dimension:

- **Social Embedding** (z_{soc}) is derived from the *visual modality* ($\bar{\boldsymbol{e}}_{\text{img}}$), as social communication deficits in autism are heavily reflected in appearance-based cues: body posture during interaction, spatial orientation toward interaction partners, head position and gaze direction proxies, and overall configurational patterns that signal social engagement or withdrawal. The SKEPXEL visual representation, enriched by ViT-extracted patch features, naturally captures these appearance-based social cues.

- **Motor Embedding** (z_{mot}) is derived from the *kinematic modality* ($\bar{\boldsymbol{e}}_{\text{skel}}$), as motor coordination deficits are most directly observable through joint kinematics: coordination patterns across multiple joints, movement smoothness (absence of jerk or abrupt changes), execution precision, and bilateral coordination. The MS-G3D-extracted joint features, which encode spatiotemporal graph patterns over the skeleton, naturally capture these kinematic coordination features.
- **Gait Embedding** (z_{gait}) is also derived from the *kinematic modality* ($\bar{\boldsymbol{e}}_{\text{skel}}$), but focuses on locomotion-specific patterns: stride length and width, bilateral symmetry between left and right limbs, rhythmic periodicity of stepping motions, and postural stability during walking. While both motor control and gait are extracted from the same kinematic modality, they are projected through *separate, independently parameterized MLPs* (f_{mot} and f_{gait}), allowing the model to learn distinct latent representations that emphasize different aspects of the kinematic signal. This separation operationalizes the theoretical distinction between general motor coordination capabilities and specific locomotion patterns.

This modality-construct alignment is grounded in clinical practice: during ADOS assessments, clinicians observe social communication primarily through visual appearance and behavioral context, while motor and gait characteristics are assessed through observation of movement execution and patterns. Our architecture mirrors this observational structure.

3.5.3. Learnable Theory Weights: Interpretable Instance-Specific Fusion A critical innovation in our design is the computation of *instance-specific, interpretable theory weights* that indicate the relative contribution of each theoretical construct to the predicted severity for each individual. This design acknowledges the well-documented heterogeneity in autism symptom profiles: different individuals exhibit different patterns of strengths and deficits across social, motor, and gait domains. Rather than applying a fixed, population-level fusion rule, our model learns to adaptively weight the three latent channels based on the specific behavioral patterns observed in each case.

Weight Computation. We concatenate the three latent vectors to form a joint representation: $z = [z_{\text{soc}}; z_{\text{mot}}; z_{\text{gait}}] \in \mathbb{R}^{3d_z}$. From this concatenated vector, we compute theory weight logits via a small MLP $g(\cdot)$: $\boldsymbol{u} = g(z) \in \mathbb{R}^3$, where $\boldsymbol{u} = [u_{\text{soc}}, u_{\text{mot}}, u_{\text{gait}}]^\top$ are raw, unnormalized scores for each theory channel.

To obtain interpretable, normalized weights, we apply softmax normalization with a temperature τ:

$$\boldsymbol{\alpha} = \mathrm{softmax}(\boldsymbol{u}/\tau) = \left[\frac{\exp(u_{\mathrm{soc}}/\tau)}{\sum_k \exp(u_k/\tau)}, \frac{\exp(u_{\mathrm{mot}}/\tau)}{\sum_k \exp(u_k/\tau)}, \frac{\exp(u_{\mathrm{gait}}/\tau)}{\sum_k \exp(u_k/\tau)} \right]^\top \triangleq [\alpha_{\mathrm{soc}}, \alpha_{\mathrm{mot}}, \alpha_{\mathrm{gait}}]^\top, \tag{6}$$

where τ is a hyperparameter that controls the smoothness of the weight distribution. A higher τ produces more uniform weights, while lower τ produces more peaked, selective weights. The resulting weight vector $\boldsymbol{\alpha}$ satisfies $\alpha_i \geq 0$ and $\sum_i \alpha_i = 1$, making it directly interpretable as a probability distribution over theory channels. For example, if a particular individual's behavioral patterns yield $\alpha_{\mathrm{gait}} = 0.6$, $\alpha_{\mathrm{mot}} = 0.3$, $\alpha_{\mathrm{soc}} = 0.1$, this indicates that gait abnormalities are the strongest predictor of severity for this individual, with motor coordination deficits playing a secondary role and social communication deficits being less prominent. Such interpretable decompositions can support clinical hypothesis generation, personalized assessment, and identification of subgroups with distinct symptom profiles.

3.5.4. Final Fusion and Severity Prediction The final prediction combines a learned nonlinear interaction term with an interpretable theory-weighted mixture: $\boldsymbol{h} = \phi(\boldsymbol{z}) + \alpha_{\mathrm{soc}}\boldsymbol{z}_{\mathrm{soc}} + \alpha_{\mathrm{mot}}\boldsymbol{z}_{\mathrm{mot}} + \alpha_{\mathrm{gait}}\boldsymbol{z}_{\mathrm{gait}} \in \mathbb{R}^{d_z}$, where $\phi(\cdot)$ is an MLP operating on the concatenated latent vector $\boldsymbol{z}$ to learn nonlinear interactions among the three theory channels. This additive combination balances two complementary fusion mechanisms:

- The *interaction term* $\phi(\boldsymbol{z})$ captures complex, nonlinear relationships among the three symptom dimensions. For example, certain combinations of social and motor deficits may have synergistic effects on overall severity that are not simply additive. This term provides the model with flexibility to learn data-driven fusion rules that may not align perfectly with theory.
- The *weighted mixture* $\sum_i \alpha_i \boldsymbol{z}_i$ enforces an interpretable, theory-consistent fusion structure. Each theory channel contributes to the final representation proportionally to its learned weight, making the fusion process transparent and explainable. This term ensures that the model's predictions can be decomposed into theory-aligned components.

Finally, we produce the severity prediction $\hat{y}$ via a linear regression head. Our training objective is to minimize the mean squared error between predicted and ground-truth ADOS total scores: $\mathcal{L} = \frac{1}{N}\sum_{i=1}^{N}(\hat{y}_i - y_i)^2$. which is a standard objective for continuous regression tasks. N is the number of training samples, $\hat{y}_i$ is the model's predicted severity for sample i, and y_i is the ground-truth ADOS total score.

4. Experiment Setup

4.1. Dataset

We evaluate our model using the DREAM dataset (Billing et al. 2020), a publicly released dataset collected in the context of structured clinical interactions with children diagnosed with autism spectrum disorder. The dataset was designed to support data-driven analysis of autism-related behaviors under strict privacy constraints. As raw video and audio recordings of children cannot be released, the dataset provides skeletal joint trajectories derived from multimodal sensing during standardized assessment sessions.

The dataset includes 61 children between the ages of 3 and 6, each assessed using the Autism Diagnostic Observation Schedule. For each child, multiple assessment sessions are available, yielding a total of 3,121 skeletal sequences. Each sequence is treated as an individual sample, paired with the corresponding ADOS total score. This setting reflects realistic clinical constraints, in which repeated observations of the same individual may be available but labels are obtained at the subject level.

Given the limited size of the DREAM dataset (common in clinical research), we employ *k-fold cross-validation* to obtain robust estimates of model performance and reduce the impact of dataset-specific variability. The full dataset is partitioned into $k = 10$ folds, and the training and testing procedure is repeated k times. Final performance metrics are reported as the mean across all folds.

4.2. Baseline Methods

To contextualize the performance of our proposed theory-driven multimodal architecture, we compare against multiple categories of baseline approaches:

Traditional Machine Learning with Handcrafted Features. These baselines represent feature-engineering approaches common in clinical informatics. We extract a comprehensive set of handcrafted features from skeleton sequences, including: joint angle statistics, movement velocity and acceleration distributions, bilateral symmetry indices (left-right coordination), postural stability measures (center-of-mass variance), and gait-specific parameters (stride length, step width, cadence). Three classical regressors are trained on these features: (1) XGBoost, (2) Random Forest, and (3) Support Vector Regression (SVR).

Single-Modality Deep Learning Approaches. These baselines process either visual or kinematic data in isolation, testing whether multimodal integration is necessary. (4) *ViT-Only*: A vision transformer pretrained

on ImageNet processes SKEPXEL pseudo-images, followed by a regression head. (5) *MS-G3D-Only*: A Multi-Scale Graph Convolutional Network (Liu et al. 2020) pretrained on skeleton-based action recognition processes skeleton sequences, followed by a regression head.

Multimodal Baselines. (6) *Established Multimodal ADOS Baseline*: This baseline concatenates features from frozen ViT and MS-G3D encoders (the same backbones used in our approach) and passes the concatenated vector through a simple feedforward network for regression. This method represents the current state-of-the-art autism analysis approach based on skeletal joint trajectories, proposed by Zahan et al. (2023). Comparing against this state-of-the-art baseline isolates the contribution of our architectural innovations, including cross-attention and theory-guided fusion, beyond simply using multimodal data, demonstrating whether sophisticated integration mechanisms provide value over straightforward feature concatenation. (7) *Medical Vision–Language Foundation Model (MedGemma)*: Recent medical vision–language foundation models have shown strong performance across a range of clinical perception and reasoning tasks. To evaluate whether such general-purpose medical VLMs can serve as competitive alternatives to domain-specific multimodal architectures, we include MedGemma (Sellergren et al. 2025). In this setup, SKEPXEL pseudo-images are paired with a templated textual prompt describing the assessment task, and the MedGemma vision–language encoder is used to produce a ADOS prediction.

Ablation Variants. To isolate specific design choices in our architecture, we compare against ablated versions of our full model: (8) *Bidirectional Cross-Attention*: Enables both skeleton-to-image and image-to-skeleton attention, testing whether unidirectional flow is superior. (9) *Skeleton-to-Image Cross-Attention*: Reverses the query direction, testing attention directionality. (10–12) *Theory Component Ablations*: Variants with social communication, motor control, or gait analysis modules removed, testing each component's contribution. (13–15) *Fusion Design Ablations*: Variants with early fusion, fixed theory weights, or no alignment mask, testing fusion mechanism choices.

4.3. Evaluation Metrics

Consistent with clinical assessment requirements and machine learning best practices, we evaluate model performance using three complementary metrics that capture distinct facets of performance:

Mean Absolute Error (MAE). MAE measures the average magnitude of prediction errors in ADOS total scores, providing a direct interpretation in clinically meaningful units. Lower MAE indicates more accurate predictions.

Pearson Correlation Coefficient. Pearson correlation measures the strength and direction of the linear relationship between predicted and actual severity scores. Pearson correlation ranges from -1 to 1, with values closer to 1 indicating stronger positive linear association.

Quadratic Weighted Kappa (QWK). QWK measures agreement between predicted and actual severity categories when continuous scores are binned into ordinal classes, with quadratic penalties for larger disagreements. For autism assessment, following the standardized ADOS calibrated severity score methodology (Gotham et al. 2009), we bin predicted and actual ADOS total scores into three clinically meaningful diagnostic categories based on age and evaluation module: *Non-Spectrum* (NS), *Autism Spectrum Disorder* (ASD), and *Autistic* (AUT, representing the most severe presentation). This classification accounts for developmental differences across age groups and assessment contexts, providing a more clinically valid categorization than arbitrary score cutoffs. QWK ranges from -1 to 1, with 1 indicating perfect agreement and 0 indicating agreement no better than chance. This metric is particularly relevant for clinical practice, where distinguishing between non-spectrum, ASD, and autistic presentations is more critical than precise score prediction, as these categories directly inform diagnostic conclusions and intervention intensity levels.

The three metrics jointly provide a comprehensive evaluation. MAE quantifies absolute accuracy (critical for score-based diagnosis), Pearson correlation captures rank ordering (critical for population stratification and resource allocation), and QWK measures categorical agreement (critical for severity-based intervention planning). A model that performs well across all three metrics demonstrates robust predictive utility suitable for clinical decision support systems. Reporting all three metrics also guards against overfitting to a single objective and provides multiple perspectives on model performance aligned with different clinical use cases.

5. Results

5.1. Comparison with Baseline Methods

We begin by establishing whether our theory-driven model architecture delivers tangible performance improvements over baseline approaches. We compare our model against three categories of baselines representing the current state of practice: traditional machine learning methods based on handcrafted kinematic

features, single-modality deep learning models that process either visual or skeletal data in isolation, established multimodal models for autism severity prediction, and a large medical vision–language foundation model (MedGemma) that provides implicit multimodal alignment through large-scale pretraining. Table 1 summarizes the comparative results.

Table 1 Performance Comparison with Baseline Methods

Method	MAE ↓	Pearson ↑	QWK ↑
Traditional ML			
XGBoost	2.514	0.507	0.297
Random Forest	2.562	0.485	0.234
SVR	2.686	0.364	0.223
Single-Modality Approaches			
ViT-Only (SKEPXEL)	2.936	0.138	0.028
MS-G3D-Only (Skeleton)	2.703	0.414	0.214
Multimodal Approaches			
Multimodal Autism (Zahan et al. 2023)	2.550	0.479	0.355
MedGemma (Sellergren et al. 2025)	4.591	0.002	0.017
Our Proposed Method			
Ours	**2.379**	**0.533**	**0.441**

Our proposed model demonstrates substantial improvements over all baseline methods across all three evaluation metrics. When compared to traditional machine learning approaches using handcrafted features, our method achieves consistent gains: MAE reductions of 5.4%, 7.1%, and 11.4% relative to XGBoost, Random Forest, and SVR respectively. More notably, our model attains a QWK of 0.441 compared to XGBoost's 0.297, corresponding to a 48.5% relative improvement. This indicates substantially stronger agreement with clinically meaningful severity categories, which is particularly relevant for downstream screening and intervention planning. These gains suggest that pretrained representation learning captures hierarchical and subtle behavioral patterns that are difficult to encode through manually designed features, and that theory-guided fusion in learned latent spaces enables more nuanced integration than is possible with fixed feature sets.

Relative to single-modality approaches, our method achieves 19.0% and 12.0% MAE reductions compared to ViT-Only and MS-G3D-Only respectively, with Pearson correlation improvements of 286.2% and 28.7%. The particularly weak correlation of the ViT-Only model indicates that visual appearance cues alone provide

insufficient signal for reliable severity estimation. Skeleton-based modeling performs better, reflecting the relevance of motor and kinematic patterns, but still underperforms the multimodal setting. These results support the view that autism-related behavioral severity reflects a combination of observable social cues and underlying movement dynamics, neither of which is adequately captured in isolation.

The comparison with the established multimodal autism assessment model of Zahan et al. (2023) is especially informative, which concatenates ViT and MS-G3D features without cross-attention or theory-guided integration. While this naive multimodal approach (MAE=2.550, Pearson=0.479, QWK=0.355) outperforms individual unimodal methods, it remains inferior to our theory-driven architecture. Our model achieves a 6.7% reduction in MAE (2.379 vs. 2.550), an 11.3% improvement in Pearson correlation (0.533 vs. 0.479), and a 24.2% improvement in QWK (0.441 vs. 0.355). These gains demonstrate that performance improvements arise not merely from combining modalities, but from how they are integrated. Cross-attention enables adaptive, semantically aligned interaction between modalities, while theory-guided fusion imposes clinically grounded structure that mitigates reliance on spurious correlations in high-dimensional concatenated feature spaces.

Finally, we observe that the large medical vision–language foundation model MedGemma performs poorly on this task, with near-zero correlation and substantially higher error across all metrics. This result highlights an important limitation of general-purpose medical VLMs for fine-grained behavioral assessment. Although MedGemma benefits from large-scale multimodal pretraining, its representations are optimized for broad clinical perception and reporting tasks rather than subtle temporal, kinematic, and interactional patterns that characterize autism severity. The large performance gap suggests that a powerful medical generative AI model alone is insufficient for this domain, and that task-specific architectural design and domain theory remain critical for accurate autism behavioral modeling.

5.2. Contribution of Theory-Guided Components

Having established the model's overall performance advantage, we next examine whether this utility is achieved in a *theory-consistent* manner. Specifically, do the theoretical constructs we have operationalized (social communication deficits, motor control impairments, and gait abnormalities) provide measurable incremental value beyond generic multimodal learning?

We conduct systematic ablation studies, removing each theoretical component while holding the architecture constant. Table 2 presents performance when each theory module is ablated.

Table 2 Contribution Analysis of Theory-Guided Components

Configuration	MAE ↓	Pearson ↑	QWK ↑
Without Social Communication	2.463	0.500	0.421
Without Motor Control	2.511	0.488	0.427
Without Gait Analysis	2.442	0.503	0.428
Ours (All Theories)	**2.379**	**0.533**	**0.441**

All three theoretical components contribute meaningfully to predictive performance, with each removal causing measurable degradation. The social communication module shows the smallest performance drop when removed (MAE increases 3.5%, Pearson decreases 6.2%, QWK decreases 4.5%). This might appear counterintuitive given that social communication deficits define autism diagnosis (Guha 2014), but the result reflects an information property of our setting: the current data modalities do not include facial expression, voice, or conversational content, which are primary channels through which social communication deficits manifest clinically. This limits the incremental contribution of the social module beyond what body-level visual features already provide. Nevertheless, the substantial Pearson reduction of 6.2% indicates that the module still adds value by imposing structured and interpretable latent representations.

The motor control component demonstrates a more substantial contribution, with removal increasing MAE by 5.5% and reducing Pearson correlation by 8.4%. This finding aligns with emerging evidence that motor impairments are not merely comorbid but core features systematically linked to autism severity (Fournier et al. 2010, MacDonald et al. 2013). While visual features encode movement appearance, they provide limited access to movement dynamics such as smoothness, coordination, and temporal execution. The motor control module addresses this gap by projecting kinematic features into a motor-specific latent space that captures these dynamic properties in a manner complementary to visual information. From a clinical perspective, this result suggests that computational assessment systems should attend to motor patterns even when they are not part of formal diagnostic criteria, as motor behaviors may reflect underlying neurological differences relevant to both motor and social-cognitive function.

The removal of the gait component increases MAE by 2.6%, decreases Pearson by 5.6%, and decreases QWK by 2.9%. These degradations are meaningful given that gait abnormalities are *not* part of standard assessment protocols like ADOS. The empirical contribution of the gait module supports emerging work suggesting that locomotion patterns, including step width variability, bilateral asymmetry, and stride rhythmicity (Esposito et al. 2011, Kindregan et al. 2015), may serve as behavioral biomarkers for autism. By isolating gait from general motor control, our architecture tests whether locomotion-specific features provide incremental value beyond coordination measures, and the ablation confirms they do. This exemplifies how theory-driven computational artifacts can *discover and validate* new clinical insights of the gait module's contribution, suggesting these patterns contain diagnostic signal that traditional methods fail to capture.

Together, the complementary contributions of all three components support the multidimensional view of autism that motivates our design. Severity is not explained by a single factor but reflects interacting differences across social, motor, and gait domains. The learnable theory weights enable adaptive integration of these domains in a way that reflects individual variability.

5.3. Comparison with Alternative Fusion Designs

Ablation studies establish that individual theory components contribute, but do not fully isolate the *fusion mechanism*'s contribution. To address this, we compare against three alternatives controlling for model capacity while varying fusion design: (1) early fusion, which concatenates features before theory-specific processing, (2) concatenation fusion, which combines modality features through late-stage concatenation, and (3) fixed fusion, which uses uniform weights rather than learning instance-specific theory weights. Table 3 summarizes the results.

Table 3 Comparison with Alternative Multimodal Fusion Designs

Fusion Strategy	MAE ↓	Pearson ↑	QWK ↑
Early Fusion	2.809	0.314	0.135
Concatenation Fusion	2.840	0.277	0.108
Fixed Fusion	2.476	0.487	0.400
Ours (Theory-Guided Fusion)	**2.379**	**0.533**	**0.441**

Early fusion, which simply concatenates visual and skeletal features before passing them through a shared network, performs dramatically worse (MAE 18.1% higher, Pearson 41.1% lower, QWK 69.4% lower).

Similarly, concatenation fusion, which combines modality features through late-stage concatenation without cross-modal attention, performs worst among all alternatives (MAE 19.4% higher, Pearson 48.0% lower, QWK 75.5% lower). These large gaps expose fundamental limitations of naive concatenation strategies. First, concatenation-based methods ignore semantic relationships between modalities. Simply stacking patch and joint embeddings provides no structural guidance regarding which visual features should interact with which kinematic features, forcing the model to infer correspondences from limited data. Second, these approaches lack a mechanism for adaptive integration, applying identical fusion patterns to all inputs and ignoring individual variation in symptom profiles. In contrast, our cross-attention explicitly models correspondences through query key interactions, adaptively reweights features, and supports instance-specific fusion through learnable theory weights.

The fixed-fusion variant, using uniform weights ($\alpha_{\text{soc}} = \alpha_{\text{mot}} = \alpha_{\text{gait}} = 1/3$) rather than learning weights, also underperforms (MAE increases 4.1%, Pearson decreases 8.6%, QWK decreases 9.3%). This comparison isolates the contribution of weight adaptivity and supports a key theoretical premise: autism severity is heterogeneous across individuals, with different symptom profiles emphasizing different dimensions. Some individuals exhibit pronounced social difficulties with relatively preserved motor function, while others show severe motor impairments with milder social challenges. Fixed weighting cannot represent this heterogeneity and therefore produces suboptimal predictions for individuals who deviate from population averages. In contrast, learnable weights enable dynamic adjustment based on observed behavioral patterns, yielding personalized symptom profiles that improve both predictive accuracy and interpretability.

Overall, these comparisons demonstrate that the observed performance gains arise not from generic model complexity, but from specific design choices, namely cross-attention for modeling semantic correspondence and learnable theory weights for capturing individual heterogeneity.

5.4. Impact of Alignment Mask Design

Next, we examine a key design choice within the cross-attention module, namely whether explicitly modeling joint to patch correspondence through an alignment mask improves cross-modal alignment and downstream prediction. Broadly, three approaches can be used to establish correspondence between skeleton joints

and image patches. A purely data-driven approach applies no constraints, allowing the model to learn arbitrary attention patterns from data alone. While flexible, this strategy is prone to spurious correlations when training data are limited. A fixed anatomical prior approach predefines which joints attend to which image regions based on body structure, for example restricting hand joints to attend only to hand-region patches. This approach is interpretable but rigid, and it cannot adapt to individual variation or capture unexpected yet informative cross-region dependencies. A third approach introduces a learnable structural bias that initializes correspondences using anatomically plausible priors while allowing them to be refined through gradient-based learning. This strategy balances domain knowledge with data-driven adaptation. Our learnable alignment mask follows this third approach by encoding soft correspondence priors that bias attention toward anatomically plausible alignments while remaining adjustable during training. We compare three configurations: no alignment mask, fixed alignment mask, and learnable alignment mask. Results are shown in Table 4.

Table 4 Impact of Alignment Mask Design on Model Performance

Alignment Strategy	MAE ↓	Pearson ↑	QWK ↑
No Alignment Mask	2.442	0.504	0.416
Fixed Alignment Mask	2.459	0.491	0.412
Ours (Learnable Alignment Mask)	**2.379**	**0.533**	**0.441**

The learnable alignment mask achieves the best performance across all metrics. Compared to the no-mask and fixed-mask variants, MAE is reduced by 2.6 to 3.3 percent, Pearson correlation is increased by 5.8 to 8.6 percent, and QWK is increased by 6.0 to 7.0 percent. Notably, the fixed anatomical mask performs worse than the no-mask configuration. This behavior can be explained by the construction of SKEPXEL representations, which transform skeleton sequences into pseudo-images using superpixel encoding that prioritizes spatiotemporal compactness rather than strict anatomical alignment. While spatial proximity remains semantically meaningful, the resulting patch layout does not correspond one-to-one with anatomical topology. As a result, fixed priors that assume specific joints always map to specific patches may impose incorrect correspondences that hinder learning. In contrast, the learnable mask treats alignment as a hypothesis to

be refined rather than a constraint to be enforced, allowing the model to discover semantically meaningful correspondences in the learned feature space through backpropagation.

The no-mask configuration performs between the fixed and learnable variants. This indicates that while attention mechanisms can discover useful correspondences without explicit guidance, they typically require more data and may converge to suboptimal solutions. Introducing a learnable alignment mask provides inductive bias that guides attention toward plausible structures while preserving flexibility for task-specific adaptation.

Overall, these results show that domain-knowledge-informed model design can guide learning effectively when implemented in a flexible manner. Fixed priors risk imposing incorrect structure when assumptions do not align with the data, while purely data-driven learning lacks guidance and may converge inefficiently. Learnable structural priors combine the advantages of both approaches by integrating anatomical intuition with data-driven refinement.

5.5. Impact of Cross-Attention Direction

The final design choice we examine concerns a boundary condition often under-specified in multimodal attention: the *directionality* of information flow. When integrating two modalities via cross-attention, which should "query" the other? Should visual features query kinematic (image-to-skeleton), kinematic query visual (skeleton-to-image), or both (bidirectional)? Table 5 reports results for these three configurations.

Table 5 Performance Comparison of Cross-Attention Direction Configurations

Configuration	MAE ↓	Pearson ↑	QWK ↑
Bidirectional (Skel↔Img)	2.432	0.497	0.423
Unidirectional (Skel→Img)	2.511	0.479	0.402
Ours (Unidirectional, Img→Skel)	**2.379**	**0.533**	**0.441**

The results show a clear ordering. Image-to-skeleton attention achieves the best performance, with MAE of 2.379, Pearson correlation of 0.533, and QWK of 0.441. Bidirectional attention performs second best, with MAE of 2.432, Pearson of 0.497, and QWK of 0.423. Skeleton-to-image attention performs worst, with MAE of 2.511, Pearson of 0.479, and QWK of 0.402. Relative to the bidirectional configuration, image-to-skeleton improves MAE by 2.2%, Pearson correlation by 7.2%, and QWK by 4.2%. In contrast, skeleton-to-image

degrades performance by 3.3% in MAE, 3.6% in Pearson, and 5.1% in QWK. These results confirm that attention directionality materially affects performance and that visual-to-kinematic information flow is most effective for autism severity prediction.

Three complementary factors help explain the superiority of image-to-skeleton attention. First, representational richness differs across modalities. Visual features derived from SKEPXEL encode global contextual information such as body posture, spatial relationships, and overall configuration, whereas kinematic features encode local, joint-level motion patterns. When image patches query skeleton joints, attention effectively conditions local kinematic signals on global visual context. This mirrors clinical reasoning, where movement interpretation depends on surrounding posture and scene context. Reversing the direction weakens this asymmetry, as local kinematics provide limited context for interpreting global visual structure. Second, unidirectional attention offers implicit regularization. The image-to-skeleton configuration uses fewer parameters. This reduced complexity is beneficial for small clinical datasets. The intermediate performance of bidirectional attention suggests that although symmetric information exchange is theoretically appealing, the added complexity does not translate into improved generalization and may instead increase overfitting risk. Third, semantic redundancy arises in the skeleton-to-image configuration. SKEPXEL representations are constructed from skeleton data, producing pseudo-images that encode kinematic information. When skeleton joints query image patches, the model may effectively retrieve transformed versions of information originating from the same source, resulting in circular or redundant information flow. In contrast, image-to-skeleton attention allows ViT-enriched visual features to provide complementary contextual information to MS-G3D-enriched kinematic representations, leading to more informative fusion.

6. Interpretability Analysis

Beyond predictive accuracy, a central contribution of our theory-driven architecture is the transparency it affords for clinical interpretation. Unlike conventional deep learning models that produce opaque predictions, our model explicitly exposes the theory weights $\boldsymbol{\alpha} = [\alpha_{\text{soc}}, \alpha_{\text{mot}}, \alpha_{\text{gait}}]^\top$ as interpretable outputs that decompose each prediction into clinically meaningful behavioral dimensions. In this section, we examine these learned theory weights across the study population, demonstrating how they (1) provide transparent, instance-specific explanations that can support clinical decision-making, and (2) enable empirical testing of theoretical hypotheses about autism symptom heterogeneity.

6.1. Transparency and Explainability

A fundamental challenge in deploying machine learning for clinical decision support is the "black box" problem: clinicians are reluctant to trust predictions they cannot understand or verify. Our architecture addresses this challenge through interpretability-by-design, exposing the theory weights as a decomposed explanation of each prediction in terms of symptom dimensions that clinicians already use in their assessments.

For any individual, the theory weight vector $\boldsymbol{\alpha}$ indicates the relative contribution of social, motor, and gait dimensions to the predicted severity score. They form a probability distribution over the three behavioral domains, enabling direct interpretation as a "symptom profile." A clinician reviewing a model prediction can inspect these weights to understand *why* the model predicts a certain severity level and *which* behavioral domains are most indicative for that particular individual.

The first row of Figure 2 presents the distribution of learned theory weights across all individuals in the dataset. Several observations emerge from this analysis. First, the model learns non-trivial weight distributions that vary across individuals, confirming that the architecture successfully captures heterogeneity in symptom presentations rather than collapsing to a fixed, population-level fusion rule. Second, all three behavioral domains receive substantial weight on average, with motor control (mean $\alpha_{\text{mot}} = 0.348$) and gait (mean $\alpha_{\text{gait}} = 0.347$) showing slightly higher average contributions than social communication (mean $\alpha_{\text{soc}} = 0.305$). This pattern suggests that kinematic features extracted from skeleton sequences carry particularly strong predictive signals for autism severity in this dataset, consistent with the growing clinical literature emphasizing motor abnormalities as core features of autism rather than mere comorbidities.

Third, the weight distributions exhibit moderate variability, indicating that while the model maintains stable overall preferences across the population, it meaningfully differentiates individuals. The ranges of observed weights (social communication spanning [0.259, 0.334], motor control spanning [0.322, 0.385], and gait spanning [0.319, 0.379]) demonstrate that no single domain completely dominates predictions, and that the model learns to balance multiple behavioral dimensions in a data-driven manner.

This transparency has direct implications for clinical workflows. When reviewing a model prediction, clinicians can evaluate whether the inferred symptom profile aligns with their own observations during

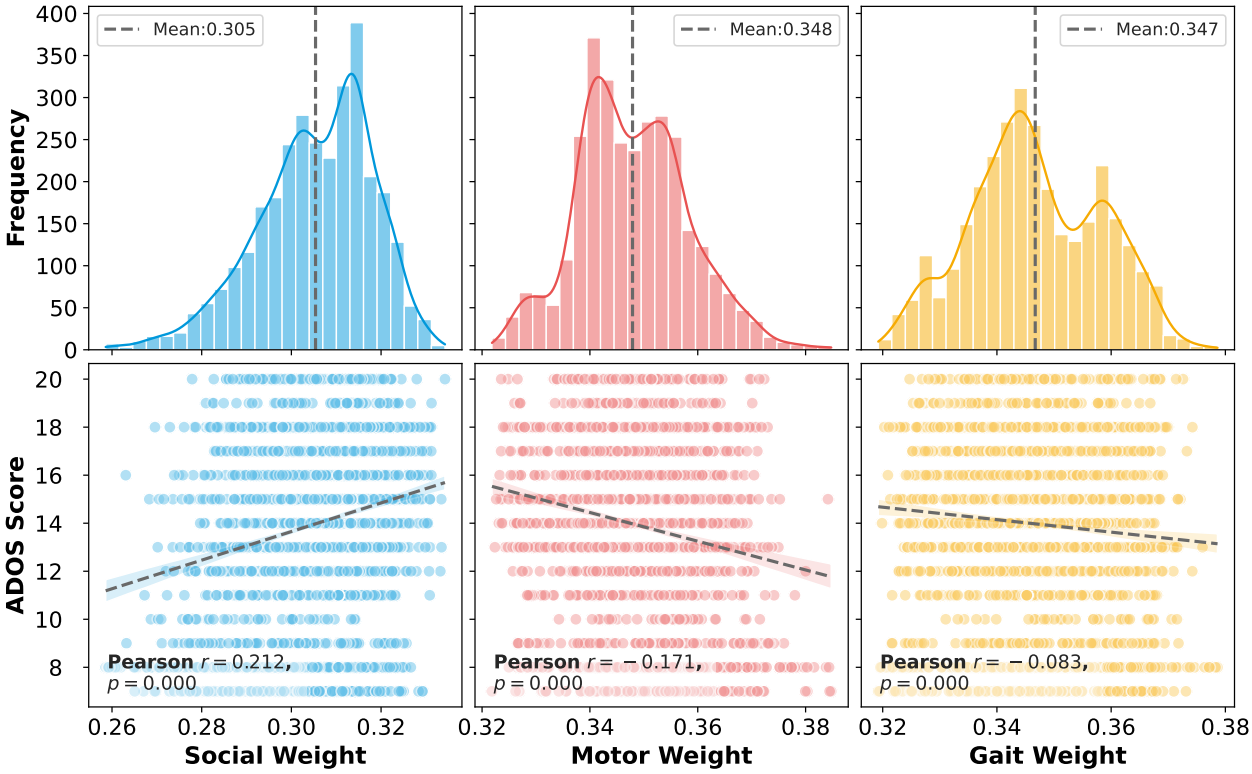

Figure 2 **Learned theory weights and their relationship to symptom severity across behavioral domains. The first row shows the distribution of learned theory weights across all individuals for each domain (social, motor, and gait), illustrating meaningful inter-individual variation with overall stability. The second row shows the relationship between learned theory weights and ADOS total scores, including scatter plots and correlations for each domain.**

assessment. For example, if the model assigns high weight to gait abnormalities for an individual, the clinician can verify whether gait irregularities were indeed prominent during observation. This process supports appropriate trust calibration: agreement may increase clinicians' confidence in the prediction, whereas discrepancies can prompt their closer examination of the implicated behavioral domains.

6.2. Theory Testing and Symptom Heterogeneity

Beyond supporting individual-level interpretation, the learned theory weights enable population-level analyses that can test theoretical hypotheses about autism symptomatology. A central tenet of contemporary autism research is that the condition is characterized by marked heterogeneity: different individuals exhibit different constellations of symptoms across behavioral domains, and this heterogeneity may have impli-

cations for etiology, prognosis, and intervention design (Lombardo et al. 2019, Litman et al. 2025). Our model's explicit theory weights provide a quantitative lens for examining this heterogeneity.

The second row of Figure 2 examines the relationship between theory weights and overall autism severity as measured by ADOS total scores. The analysis reveals statistically significant correlations for all three behavioral domains, each with distinct patterns that invite theoretical interpretation. Social communication weights exhibit a significant positive correlation with severity (Pearson $r = 0.21$, $p < 0.001$): individuals with higher ADOS total scores tend to receive higher weight on the social communication channel. This finding aligns with the clinical centrality of social communication deficits in autism diagnosis (Lord et al. 2000, Chevallier et al. 2012), as the ADOS assessment protocol places substantial emphasis on social-communicative behaviors. As severity increases, social communication impairments become more prominent relative to motor abnormalities, and the model's learned weights capture this clinical pattern.

Conversely, motor control weights show a significant negative correlation with severity ($r = -0.17$, $p < 0.001$), as do gait weights ($r = -0.08$, $p < 0.001$). These negative correlations suggest that for individuals with lower overall severity, kinematic abnormalities (motor control and gait) play a relatively larger role in the model's predictions. One interpretation is that motor abnormalities may serve as particularly salient biomarkers for individuals at the milder end of the autism spectrum, where social communication deficits may be subtler and harder to detect. This hypothesis is consistent with emerging research suggesting that motor signatures may be among the earliest detectable signs of autism and may remain prominent even when social symptoms are less severe (Esposito et al. 2011, Lum et al. 2021).

These findings have implications for both clinical practice and theoretical understanding. From a clinical perspective, the differential weighting patterns suggest that assessment strategies might benefit from tailoring emphasis based on suspected severity level. For individuals suspected of milder autism, careful attention to motor patterns and gait abnormalities may be particularly informative, whereas for individuals with more severe presentations, social communication deficits may be the most discriminative features. From a theoretical perspective, the learned weights provide empirical evidence for the multidimensional, heterogeneous nature of autism symptomatology, validating the appropriateness of decomposing severity prediction into distinct behavioral channels.

6.3. Implications for Clinical Subtyping

The theory weights also enable data-driven identification of symptom-based subgroups. Traditional autism subtyping has largely relied on categorical diagnostic labels or expert-defined clusters, whereas the continuous weight vectors learned by our model provide a complementary quantitative alternative. Individuals with similar weight profiles, for example those with consistently elevated gait weights, may form behaviorally coherent subgroups that share common underlying characteristics.

Such subtyping has potential clinical utility. If certain subgroups consistently show elevated weights for particular behavioral domains, this may suggest that those domains are particularly salient biomarkers for those individuals, with implications for personalized intervention design. For instance, individuals in a "high-gait-weight" subgroup might benefit particularly from interventions targeting locomotion and postural control, while individuals in a "high-social-weight" subgroup might benefit more from social skills training. While our current analysis does not exhaustively explore subgroup identification, the architecture's transparent weight outputs provide the foundation for such future investigations.

Moreover, the theory weights could be analyzed in conjunction with other clinical measures and demographic variables to test hypotheses about symptom heterogeneity. Do theory weights correlate with age, gender, cognitive ability, or co-occurring conditions? Are certain weight profiles associated with particular genetic variants or neuroimaging findings? Such analyses, enabled by our interpretable architecture, could contribute to the broader scientific goal of parsing autism heterogeneity into meaningful subtypes with distinct etiological and clinical profiles.

6.4. Limitations and Considerations

Several limitations should be acknowledged when interpreting the theory weight analyses. First, the correlations between theory weights and ADOS total scores, while statistically significant, are modest in magnitude (absolute $|r|$ values ranging from 0.08 to 0.21). This suggests that while systematic relationships exist, substantial individual variability remains unexplained by severity score alone. Such variability is expected given the heterogeneous nature of autism and is precisely what motivates the instance-specific weight computation.

Second, the theory weights are optimized to minimize prediction error, not to maximize clinical interpretability per se. While the architecture encourages interpretable decomposition through its structure, the

learned weights ultimately reflect whatever patterns best predict the target ADOS total score. If certain behavioral dimensions happen to be noisy or unreliably measured in the dataset, their weights may not accurately reflect their true clinical importance. Cross-validation across datasets and assessment protocols would strengthen confidence in the generalizability of the observed weight patterns.

Third, the three-way decomposition into social, motor, and gait channels, while grounded in clinical theory, is not exhaustive. Autism symptomatology also encompasses sensory processing, repetitive behaviors, language patterns, and other dimensions not explicitly modeled. Future work could extend the architecture to incorporate additional theory-aligned channels, though at the cost of increased complexity and potential dilution of individual channel interpretability.

Despite these limitations, the theory weight analyses demonstrate the interpretability benefits of our theory-driven design. By exposing learned behavioral decompositions as explicit model outputs, we enable a form of transparency that pure prediction-focused models cannot provide, supporting clinical insight, hypothesis generation, and trust calibration in ways that opaque deep learning approaches do not afford.

7. Conclusion

This paper presents a novel theory-driven deep learning model for automated autism severity assessment that bridges the traditionally disparate goals of predictive accuracy and clinical interpretability. Our approach departs from conventional machine learning paradigms that treat autism as a monolithic prediction target with opaque feature representations. Instead, we design an architecture that explicitly operationalizes three clinical constructs from autism research, namely social communication deficits, motor control impairments, and gait abnormalities, as distinct computational modules within a unified deep learning framework. The architecture integrates visual features with kinematic features through a unidirectional cross-attention mechanism that enables semantically meaningful cross-modal alignment. A learnable alignment mask encodes soft priors over the correspondence between image patches and skeleton joints, while instance-specific theory weights decompose each prediction into interpretable contributions from the three behavioral domains. Empirical evaluations demonstrate that this theory-guided design achieves state-of-the-art predictive performance while simultaneously providing transparent, clinically grounded explanations that can support clinical decision-making and hypothesis generation.

The theoretical contributions of this work extend prior research on theory-driven algorithm design for healthcare applications. By encoding clinical theories as architectural components, we show how domain knowledge can be operationalized not only as input features or post-hoc interpretations, but as structural elements that shape model learning throughout training. Explicit representation of social communication, motor control, and gait as distinct latent channels enables empirical testing of theoretical hypotheses that are inaccessible to atheoretical black-box models. Ablation studies confirm that all three constructs contribute measurably to predictive accuracy, providing empirical support for the multidimensional conceptualization of autism motivating contemporary clinical research. Notably, analysis of the learned theory weights reveals systematic relationships between symptom profiles and overall severity. Social communication deficits become increasingly prominent predictors at higher severity levels, whereas motor and gait abnormalities play relatively larger roles at the milder end of the spectrum. This pattern emerges directly from the learned representations and aligns with clinical observations suggesting that motor signatures may be particularly informative biomarkers for individuals with subtler social symptom presentations. Our model therefore functions not only as a predictive model, but also as a tool for theory discovery that enables computational investigation of symptom heterogeneity informing both clinical understanding and intervention design.

The practical implications of this research span clinical assessment, intervention planning, and broader deployment of artificial intelligence in healthcare settings. The achieved performance represents substantial gains in diagnostic accuracy relative to existing methods. Beyond predictive performance, the interpretable theory weights provide clinicians with transparent explanations of model outputs in terms of symptom dimensions already used in clinical assessment. When the model assigns high weight to gait abnormalities for an individual, clinicians can verify this against their own observations, supporting appropriate trust calibration and identifying cases that may warrant closer examination. This transparency addresses a key barrier to clinical AI adoption, namely clinician reluctance to rely on predictions that cannot be understood or verified. In addition, the instance-specific symptom profiles generated by the model offer potential utility for personalized intervention planning. Individuals whose predictions are dominated by motor or gait weights may benefit from motor-focused interventions, while those with elevated social communication weights

may respond more strongly to social skills training. Although such applications require validation beyond the scope of this study, our model establishes a foundation for precision approaches that tailor intervention strategies to individual symptom profiles rather than applying uniform treatment protocols.

Several limitations of this work suggest directions for future research. The three-way decomposition into social communication, motor control, and gait, while grounded in clinical theory, is not exhaustive. Autism symptomatology also includes sensory processing differences, restricted and repetitive behaviors, language patterns, and other dimensions not explicitly modeled here. Future work could extend our model with additional theory-aligned channels, potentially informed through collaboration with clinical experts. The modest correlations between theory weights and ADOS total scores indicate that although systematic relationships exist, substantial individual variability remains unexplained, reflecting the inherent heterogeneity of autism. Moreover, the current modalities do not include voice, conversational content, or facial expression information, which are central channels through which social communication deficits manifest. Incorporating these modalities may strengthen the social communication component in future iterations. Finally, although our model provides interpretability by design through exposed theory weights, rigorous evaluation with clinical end-users is necessary to determine whether these explanations are perceived as meaningful and actionable in real-world assessment workflows.

References

Ahmed MI, Spooner B, Isherwood J, Lane M, Orrock E, Dennison A (2023) A systematic review of the barriers to the implementation of artificial intelligence in healthcare. *Cureus* 15(10).

Bae S, Hong J, Ha S, Moon J, Yu J, Choi H, Lee J, Do R, Sim H, Kim H, et al. (2025) Multimodal ai for risk stratification in autism spectrum disorder: integrating voice and screening tools. *NPJ digital medicine* 8(1):538.

Billing E, Belpaeme T, Cai H, Cao HL, Ciocan A, Costescu C, David D, Homewood R, Hernandez Garcia D, Gómez Esteban P, et al. (2020) The dream dataset: Supporting a data-driven study of autism spectrum disorder and robot enhanced therapy. *PloS one* 15(8):e0236939.

Bone D, Bishop SL, Black MP, Goodwin MS, Lord C, Narayanan SS (2016) Use of machine learning to improve autism screening and diagnostic instruments: Effectiveness, efficiency, and multi-instrument fusion. *Journal of Child Psychology and Psychiatry* 57(8):927–937.

Cao Z, Hidalgo G, Simon T, Wei SE, Sheikh Y (2019) Openpose: Realtime multi-person 2d pose estimation using part affinity fields. *IEEE transactions on pattern analysis and machine intelligence* 43(1):172–186.

Cavus N, Lawan AA, Ibrahim Z, Dahiru A, Tahir S, Abdulrazak UI, Hussaini A (2021) A systematic literature review on the application of machine-learning models in behavioral assessment of autism spectrum disorder. *Journal of Personalized Medicine* 11(4):299.

Chevallier C, Kohls G, Troiani V, Brodkin ES, Schultz RT (2012) The social motivation theory of autism. *Trends in cognitive sciences* 16(4):231–239.

Dawson G, Rogers S, Munson J, Smith M, Winter J, Greenson J, Donaldson A, Varley J (2010) Randomized, controlled trial of an intervention for toddlers with autism: the early start denver model. *Pediatrics* 125(1):e17–e23.

Dosovitskiy A, Beyer L, Kolesnikov A, Weissenborn D, Zhai X, Unterthiner T, Dehghani M, Minderer M, Heigold G, Gelly S, Uszkoreit J, Houlsby N (2021) An image is worth 16x16 words: Transformers for image recognition at scale. *International Conference on Learning Representations (ICLR)*.

Duda M, Ma R, Haber N, Wall D (2016) Use of machine learning for behavioral distinction of autism and adhd. *Translational psychiatry* 6(2):e732–e732.

Durán JM, Jongsma KR (2021) Who is afraid of black box algorithms? on the epistemological and ethical basis of trust in medical ai. *Journal of medical ethics* 47(5):329–335.

Esposito G, Venuti P, Apicella F, Muratori F (2011) Analysis of unsupported gait in toddlers with autism. *Brain and development* 33(5):367–373.

Fournier KA, Hass CJ, Naik SK, Lodha N, Cauraugh JH (2010) Motor coordination in autism spectrum disorders: a synthesis and meta-analysis. *Journal of autism and developmental disorders* 40(10):1227–1240.

Gotham K, Pickles A, Lord C (2009) Standardizing ados scores for a measure of severity in autism spectrum disorders. *Journal of autism and developmental disorders* 39(5):693–705.

Gowen E, Hamilton A (2013) Motor abilities in autism: a review using a computational context. *Journal of autism and developmental disorders* 43(2):323–344.

Guha M (2014) *Diagnostic and Statistical Manual of Mental Disorders: DSM-5 (5th edition)*. URL http://dx.doi.org/10.1108/RR-10-2013-0256.

Hashemi J, Dawson G, Carpenter KL, Campbell K, Qiu Q, Espinosa S, Marsan S, Baker JP, Egger HL, Sapiro G (2018) Computer vision analysis for quantification of autism risk behaviors. *IEEE Transactions on Affective Computing* 12(1):215–226.

Kangarani-Farahani M, Malik MA, Zwicker JG (2024) Motor impairments in children with autism spectrum disorder: A systematic review and meta-analysis. *Journal of autism and developmental disorders* 54(5):1977–1997.

Kindregan D, Gallagher L, Gormley J (2015) Gait deviations in children with autism spectrum disorders: a review. *Autism research and treatment* 2015(1):741480.

Li J, Liu S, Hu X, Zhao J, Zhao Y (2025) Drugagent: A theory-driven llm multi-agent system for automating machine learning programming in drug discovery. *Available at SSRN 5746063* URL http://dx.doi.org/10.2139/ssrn.5746063.

Lin YK, Chen H, Brown RA, Li SH, Yang HJ (2017) Healthcare predictive analytics for risk profiling in chronic care: A bayesian multitask learning approach1. *Management Information Systems Quarterly* 41(2):473–495, ISSN 0276-7783, URL http://dx.doi.org/10.25300/MISQ/2017/41.2.07.

Litman A, Sauerwald N, Green Snyder L, Foss-Feig J, Park CY, Hao Y, Dinstein I, Theesfeld CL, Troyanskaya OG (2025) Decomposition of phenotypic heterogeneity in autism reveals underlying genetic programs. *Nature Genetics* 57(7):1611–1619.

Liu J, Akhtar N, Mian A (2019) Skepxels: Spatio-temporal image representation of human skeleton joints for action recognition. *Proceedings of the IEEE/CVF Conference on Computer Vision and Pattern Recognition (CVPR) Workshops*, 10–19.

Liu Z, Zhang H, Chen Z, Wang Z, Ouyang W (2020) Disentangling and unifying graph convolutions for skeleton-based action recognition. *Proceedings of the IEEE/CVF Conference on Computer Vision and Pattern Recognition (CVPR)*, 143–152.

Lombardo MV, Lai MC, Baron-Cohen S (2019) Big data approaches to decomposing heterogeneity across the autism spectrum. *Molecular psychiatry* 24(10):1435–1450.

Lord C, Risi S, Lambrecht L, Cook Jr EH, Leventhal BL, DiLavore PC, Pickles A, Rutter M (2000) The autism diagnostic observation schedule—generic: A standard measure of social and communication deficits associated with the spectrum of autism. *Journal of autism and developmental disorders* 30(3):205–223.

Lum JA, Shandley K, Albein-Urios N, Kirkovski M, Papadopoulos N, Wilson RB, Enticott PG, Rinehart NJ (2021) Meta-analysis reveals gait anomalies in autism. *Autism Research* 14(4):733–747.

MacDonald M, Lord C, Ulrich D (2013) The relationship of motor skills and adaptive behavior skills in young children with autism spectrum disorders. *Research in autism spectrum disorders* 7(11):1383–1390.

Morid MA, Sheng ORL (2025) Healthcare cost prediction for heterogeneous patient profiles using deep learning models with administrative claims data. *Information Systems Research* 36(4):1968–1992, URL http://dx.doi.org/10.1287/isre.2021.0643.

Morrow E, Zidaru T, Ross F, Mason C, Patel KD, Ream M, Stockley R (2023) Artificial intelligence technologies and compassion in healthcare: A systematic scoping review. *Frontiers in Psychology* 13:971044.

Rudin C (2019) Stop explaining black box machine learning models for high stakes decisions and use interpretable models instead. *Nature machine intelligence* 1(5):206–215.

Rudin C, Chen C, Chen Z, Huang H, Semenova L, Zhong C (2022) Interpretable machine learning: Fundamental principles and 10 grand challenges. *Statistic Surveys* 16:1–85.

Rutter M, DiLavore P, Risi S, Gotham K, Bishop S (2012) Autism diagnostic observation schedule: Ados-2.

Sellergren A, Kazemzadeh S, Jaroensri T, Kiraly A, Traverse M, Kohlberger T, Xu S, Jamil F, Hughes C, Lau C, et al. (2025) Medgemma technical report. *arXiv preprint arXiv:2507.05201* .

Tariq Q, Daniels J, Schwartz JN, Washington P, Kalantarian H, Wall DP (2018) Mobile detection of autism through machine learning on home video: A development and prospective validation study. *PLoS medicine* 15(11):e1002705.

Wall DP, Kosmicki J, Deluca T, Harstad E, Fusaro VA (2012) Use of machine learning to shorten observation-based screening and diagnosis of autism. *Translational psychiatry* 2(4):e100–e100.

Xie J, Chai Y, Liang R, Liu Y, Zeng DD (2025) Short-form videos and mental health: A knowledge-guided neural topic model. *Information Systems Research* URL http://dx.doi.org/10.1287/isre.2024.1071.

Zahan S, Gilani Z, Hassan GM, Mian A (2023) Human gesture and gait analysis for autism detection. *Proceedings of the IEEE/CVF Conference on Computer Vision and Pattern Recognition (CVPR) Workshops*, 3328–3337.

Zhang Y, Tian Y, Wu P, Chen D (2021) Application of skeleton data and long short-term memory in action recognition of children with autism spectrum disorder. *Sensors* 21(2):411.

Zhou T, Wang Y, Yan L, Tan Y (2023) Spoiled for choice? personalized recommendation for healthcare decisions: A multiarmed bandit approach. *Information Systems Research* 34(4):1493–1512, URL http://dx.doi.org/10.1287/isre.2022.1191.

Zhu Fl, Wang Sh, Liu Wb, Zhu Hl, Li M, Zou Xb (2023) A multimodal machine learning system in early screening for toddlers with autism spectrum disorders based on the response to name. *Frontiers in Psychiatry* 14:1039293.